Uncooperative Emitter Localization Based on Joint Sensor Selection and Semidefinite Programming

Liming CAO [1], Jianzhao ZHANG [2], Yongxiang LIU [2], Yanping ZHU [1], Junquan DENG [2], Guokai CHEN [2]

[1] Nanjing University of Information Science and Technology, Nanjing, China
[2] The Sixty-Third Research Institute, National University of Defense Technology, Nanjing, China

20201249250@nuist.edu.cn, jianzhao63s@nudt.edu.cn, lyx63s@163.com, 001520@ nuist.edu.cn, jqdeng@nudt.edu.cn, guokai.chen@nudt.edu.cn

Submitted August 9, 2022 / Accepted October 25, 2022 / Online first November 7, 2022

Abstract. *Radio emitter localization based on Received Signal Strength (RSS) is promising in large-scale Internet of Things (IoT) and wireless sensor networks (WSNs) for its low hardware and computation costs. To improve its localization accuracy and reduce the system energy consumption, we propose an improved RSS localization algorithm based on the joint sensor selection and semidefinite programming (SDP). An initial position estimate is first obtained using RSSs available at a random set of sensors. A refined sensor set is then selected to complete the second estimation by analyzing the geometric structure of sensing network. Performance of the method is evaluated in terms of localization accuracy and execution time, and compared with existing methods. Extensive simulations demonstrate that the proposed approach achieves a localization accuracy of approximately 1.5 m with 8 to 10 sensors. The method outperforms the second-order cone programming (SOCP) and the least squared relative error (LSRE)-based SDP algorithms in terms of both the location and the transmit power estimation accuracy.*

Keywords

Received signal strength, sensor selection, semidefinite programming, least squared relative error

1. Introduction

Large-scale network localization techniques in 5G and beyond 5G wireless networks are essential for many Internet-of-Things (IoT), smart city and military applications, including spectrum monitoring, intelligent transportation, asset tracking and battlefield monitoring [1], [2]. Compared with methods relying on time of arrival (TOA) [3], [4], time difference of arrival (TDOA) [5], [6], or angle of arrival (AOA) [7], [8] measurements, received signal strength (RSS) based localization method features low hardware cost and low network synchronization requirement, making it suitable for large-scale IoT with resource-constrained radio sensors [9–13].

RSS-based localization includes fingerprint localization and ranging localization. The fingerprint localization is realized in two steps. Firstly, a collection of RSS values is carried out in a certain area and an RSS-fingerprint map is created to fulfill the so-called offline training phase. Secondly, in the online test phase, the actual monitored RSS is compared to the entries in the fingerprint map to estimate the emitter location. The authors in [9] and [10] matched the actually monitored RSS with the fingerprint map using commonly used machine learning models such as K-nearest neighbor, decision tree and support vector machine to perform highly accurate emitter localization. Fingerprint localization and most traditional ranging localization algorithms assume that emitter transmitting power is known. However, the power is usually unknown in an uncooperative scenario, and methods for estimating the transmit power have been rarely investigated. We focus on the scenario where both the emitter location and transmit power need to be estimated. The authors in [14] had proposed an uncooperative RSS-based localization scheme utilizing a maximum likelihood (ML) estimator. It tried to solve a non-linear and non-convex optimization problem, which is challenging in wireless sensor network (WSN) with limited computation resources. To address such an issue, Ziskind et al. [15] proposed an iterative-based algorithm to reduce the computation complexity, but the estimation result depends on the initial value used and the optimality of the algorithm cannot be guaranteed. In [16], unscented transformation (UT) and weighted least squares (WLS) methods were applied to develop a low complexity algorithm for joint estimation of location and transmit power. In [17] and [18], the ML problem was modeled as a WLS problem, and then the WLS problem was converted into a convex semidefinite programming (SDP) or second-order cone programming (SOCP) problem, which has lower computation complexity.

The above-mentioned ranging localization algorithms are based on least squares (LS) criterion, where the sum of

DOI: 10.13164/re.2022.0553

squares of the absolute errors is minimized. To obtain a formula without a logarithm term, most researchers firstly convert the conventional RSS measurement to the absolute power domain. Then, they applied a first-order Taylor series to approximate the received power. However, in the case of noise with significant shadowing effect, this approximate representation can lead to a significant increase in position estimation error. The authors in [12] and [13] converted the traditional RSS measurement model into a multiplication model without a logarithm term. Afterward, they transformed the multiplication model to a least squared relative error (LSRE) model. The LSRE model was further relaxed into an SDP problem by semidefinite relaxation (SDR). These transformations can avoid the errors introduced by the approximation of the first-order Taylor series. The above schemes still suffered from prohibitive hardware costs and power consumption due to the usage of all the sensors in the networks. Generally, some sensors in the network do not improve the estimation performance due to the restricted communication range, while increasing the system runtime and energy consumption. Thus, this paper tries to select an optimal subset of all sensors to estimate the location and transmit power with low energy and computation overhead.

Few existing LSRE-based localization algorithms take the sensor selection problem into consideration. In the uncooperative RSS-based localization, Ababneh et al. [19] pointed out that a reasonable selection of sensors was the key factor to determine the quality of the overall network estimation. In [20], the sensor selection was molded as an optimization problem that satisfied the localization error, yet without the selection feedback mechanism. Bopardikar et al. [21] proposed an alternation-free sensor selection and localization approach based on the TDOA, which had low complexity. Nevertheless, the approach did not take into account the differences among the sensors. Bel et al. [22] solved the sensor selection problem for RSS-based localization by deriving an RSS threshold depending on the total number of sensors. Then all sensors with RSS measurements above the threshold were selected. This resulted in selecting the sensors that were closest to the emitter.

In this paper, we comprehensively consider the differences among sensors, and the geometric structure to select an optimized set of sensors. To improve the localization accuracy, lower the deployment and computational complexities in large-scale WSNs, an improved RSS localization algorithm based on joint sensor selection and SDP is proposed. Main contributions of this paper are:

- Using a series of auxiliary matrices, a bivariate joint estimation model of transmit power and location is constructed. Furthermore, we design an uncooperative emitter localization algorithm based on joint sensor selection and semidefinite programming. The algorithm achieves a good localization performance via three steps, i.e., initial position estimation, sensor selection, and refined position estimation.
- A sensor selection algorithm is proposed to reduce the system runtime and improve the system efficiency by exploring the sensor network geometry structure via network area splitting, and selecting sensors relatively close to the emitter.
- Extensive simulations for different scenarios show that the proposed algorithm can achieve higher localization accuracy with less calculation time than existing SDP and SOCP optimization algorithms.

The remaining sections are structured as follows. In Sec. 2, the sensor selection problem and the RSS measurement model are presented. Subsequently, Section 3 describes RSS-based emitter localization model. Section 4 gives the proposed sensor selection algorithm in detail. The simulation results are shown in Sec. 5. Finally, Section 6 summarizes the work of this paper and gives an outlook on future research. The corresponding Cramer-Rao lower bound (CRLB) for the RSS measurement model is derived in the Appendix.

In the following, tr (.) and rank (.) represent the trace and the rank of a matrix, respectively, $[.]^{\mathrm{T}}$ denotes the transpose of a matrix. $\mathbf{I}_m$ represents the m by m identity matrix. $\|.\|$ denotes ℓ_2 norm.

2. Problem Statement and Measurement Model

In this section, we first provide a description of the sensor selection problem and the RSS measurement model.

2.1 Sensor Selection Problem

In the RSS-based localization problem, multiple spatially separated sensors capture the radiated signal from an unknown radio emitter. Typically, there is an information fusion center (FC) responsible for collecting RSS measurements, which are the input for the localization algorithm. Due to the limited communication range, the computational complexity, and the limited battery power of the sensor, it is impractical to use all sensors for localization in a sensor network [23]. Hence, the selection of sensors is necessary in a practical scenario.

We consider a representative case where there is an unknown emitter and the N fixed sensors in a 2D network. Figure 1 provides an example of network scenario. First, a few random sensors passively perform the RSS measurement and feed the measurements to FC to perform the initial location estimation. A refined set of sensors are then selected and activated to measure the RSSs from the emitter to achieve higher localization accuracy. The transmission of data is performed in two steps. Firstly, the raw signals captured are processed locally by the individual sensors and converted into RSS data. Then, the RSS data is sent to FC to obtain the emitter location. It is worth raising

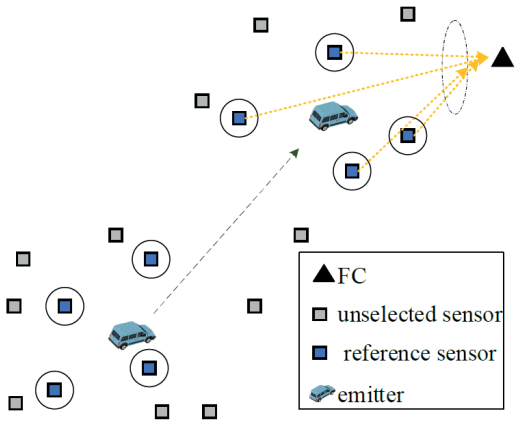

Fig. 1. Example of a sensing network.

the fact that information transmission requires energy. To reduce the overall energy consumption of the system, one sensor closest to the emitter (i.e., the sensor with the highest RSS) is selected to take on the role of FC. The FC is responsible to perform both the emitter localization and sensor selection tasks. In our assumed localization of a small area only one FC is set. However, deploying more FCs in a larger localization area is valuable to reduce localization errors.

2.2 Measurement Model

The N fixed sensor locations are denoted by $S_i = [x_i;y_i]$, $i = 1,\ldots,N$, while the emitter is denoted by $X = [a;b]$. According to the widely-used RSS measurement model [11–13], the received power (in dBm) at the i-th sensor can be modeled as:

$$P_i = P_0 - 10\beta \log_{10}\frac{d_i}{d_0} + n_i, \quad i = 1,\ldots,N \tag{1}$$

where P_0 represents the received power at the reference distance d_0, and β is the path loss exponent (PLE). $d_i = \|X - S_i\|$ represents the distance from the emitter to S_i, and n_i is the log-normal shadowing effect usually modeled as a zero-mean Gaussian distributed random variable with variance σ_i^2, i.e., $n_i \sim \mathcal{N}(0,\sigma_i^2)$.

In the case of unknown transmit power, the ML estimation problem can be expressed as [12]:

$$\arg\min_{X,P_0} \sum_{i=1}^{N} \frac{1}{\sigma_i^2}\left(P_i - P_0 + 10\beta \log_{10}\frac{d_i}{d_0}\right)^2. \tag{2}$$

3. Bivariate RSS Localization Model

The RSS of each sensor is disturbed by channel shadowing. Therefore, the sample mean is evaluated to mitigate the interference, which is given by [24]:

$$\overline{P_i} = \sum_{j=1}^{N_j} P_{i,j}/N_j \tag{3}$$

where $P_{i,j}$ represents the j-th RSS value at the i-th sensor, and N_j represents the total number of samples.

To formulate the LSRE estimation problem, the RSS measurement model in (1) is first converted into a multiplicative model. After that, we divide both sides of the model by 10β and take the power of ten, and we have [25]:

$$10^{\frac{P_0-\overline{P_i}}{10\beta}} = \|X - S_i\| 10^{-\frac{n_i}{10\beta}}. \tag{4}$$

Let $l_0 = 10^{\frac{P_0}{10\beta}}$, $l_i = 10^{-\frac{\overline{P_i}}{10\beta}}$, and $\xi_i = 10^{-\frac{n_i}{10\beta}}$, the problem (4) can be rewritten as [12]:

$$l_0 l_i = d_i \xi_i \tag{5}$$

where ξ_i represents the composite noise term. Clearly, if n_i and n_j are independent, ξ_i and ξ_j are independent for the case with $i \neq j$. The parameters to be estimated are denoted by $\hat{\theta} = \left[X^{\mathrm{T}}, P_0\right]^{\mathrm{T}}$. Motivated by [12], the LSRE-based equivalence estimation then can be formulated as:

$$\hat{\theta} = \arg\min_{X,l_0} \sum_{i=1}^{N}\left(\frac{d_i^2}{l_0^2 l_i^2} + \frac{l_0^2 l_i^2}{d_i^2}\right). \tag{6}$$

There are optimization variables both in the numerator and denominator as in (6). Therefore, problem (6) is non-convex and difficult to solve. Using traditional SDR technique cannot immediately convert the problem (6) into a standard form [13]. To apply SDR, two variables L_i and L_0 are introduced to replace $1/l_i$ and $1/l_0$ in (6), respectively. Then problem (6) is equivalent to [12], [13]:

$$\left[\hat{X}^{\mathrm{T}}, \hat{L}_0\right]^{\mathrm{T}} = \arg\min_{X,L_0} \sum_{i=1}^{N}\left(L_0^2 L_i^2 d_i^2 + \frac{1}{L_0^2 L_i^2 d_i^2}\right). \tag{7}$$

The problem (7) can be modified as [13]:

$$\min_{X,L_0} \sum_{i=1}^{N}\left(v_i + \mu_i\right), \tag{8a}$$

$$\text{s.t.} \quad L_0^2 L_i^2 d_i^2 \le v_i, \tag{8b}$$

$$\frac{1}{L_0^2 L_i^2 d_i^2} \le \mu_i \tag{8c}$$

where $v = \left[v_1,\cdots,v_N\right]^{\mathrm{T}}$ and $\mu = \left[\mu_1,\cdots,\mu_N\right]^{\mathrm{T}}$.

To decrease the complexity of obtaining unknown parameters and jointly estimate $\hat{\theta}$, a symmetric matrix z containing X is defined. $Z = z \cdot L_0^2$ is taken as a joint estimation matrix. Describing $L_0^2 d_i^2$ term in (8) with Z, we get:

$$L_0^2 \left\|X - S_i\right\|^2 = \mathrm{tr}\left(ZW_i\right), i = 1,\ldots,N \tag{9}$$

where $W_i = \begin{bmatrix} w_i & -S_i \\ -S_i^{\mathrm{T}} & 1 \end{bmatrix}_{3\times 3}$, $w_i = \begin{bmatrix} S_i^{\mathrm{T}} c_1 S_i & 0 \\ 0 & S_i^{\mathrm{T}} c_2 S_i \end{bmatrix}$, $c_1 = \begin{bmatrix} 1 & 0 \\ 0 & 0 \end{bmatrix}$, $c_2 = \begin{bmatrix} 0 & 0 \\ 0 & 1 \end{bmatrix}$, and $z = \begin{bmatrix} I_2 & X \\ X^{\mathrm{T}} & X^{\mathrm{T}} X \end{bmatrix}_{3\times 3}$.

Based on (9), the constraint problem can be written as:

$$\begin{bmatrix} v_i & \mathrm{tr}(ZW_i) \\ L_i^2 & 1 \end{bmatrix} \succeq 0, \tag{10}$$

$$\begin{bmatrix} \mathrm{tr}(ZW_i) & 1/L_i \\ 1/L_i & \mu_i \end{bmatrix} \succeq 0, \tag{11}$$

$$Z \succeq \mathbf{0}, \tag{12}$$

$$\mathrm{rank}(Z) = 2 \tag{13}$$

where $\succeq$ stands for the positive semidefinite symbol. (12) and (13) derive from the following significant equivalence:

$$Z = \begin{bmatrix} L_0^2 I_2 & L_0^2 X \\ L_0^2 X^{\mathrm{T}} & L_0^2 X^{\mathrm{T}} X \end{bmatrix}_{3\times 3} \Leftrightarrow Z \succeq 0, \mathrm{rank}(Z) = 2. \tag{14}$$

The fact that a matrix is positive semidefinite implies that problem (8) is solvable. Hence, neglecting (13), the final SDP formulation is expressed as:

$$\begin{aligned} &\min_{Z,v,\mu} \quad (8a) \\ &\text{s.t. } (10),(11),(12). \end{aligned} \tag{15}$$

With $\{Z^*, v^*, \mu^*\}$ denotes the solution to the SDP. Following the definition of Z, the location X can be calculated as:

$$\hat{X} = Z^*(1:2,3) / Z^*(1,1) \tag{16}$$

and the transmit power P_0 is obtained as:

$$\hat{P}_0 = 10\beta \log_{10}\left(1/\sqrt{Z^*(1,1)}\right). \tag{17}$$

As mentioned before, sensor selection is a problem of finding an optimized subset of sensors. To avoid the influence of the battery power of the nodes on the localization system, we assume that the power level of the nodes is sufficient. Thus, the localization accuracy heavily depends on the distances between sensors and the emitter. In sensor selection, we should consider the sensor-emitter geometry structure and its relative distance. In next section, we will investigate how to find a subset of sensors that gives positioning results with high accuracy.

4. Sensor Selection for RSS-Based Localization

4.1 Sensor Selection Scheme

The accuracy associated with the localization process relies on several factors. The main idea behind our proposed selection method is to use information of the relative location of a sensor to the emitter. On the one hand, the RSS-based localization performance is closely related to the qualities of the measured RSSs. Theoretically, the closer the sensor is to the emitter, the more effective it is in improving localization accuracy [26]. This means that the higher RSS, the more reliable the estimation results will be. On the other hand, the objective function of ML is non-linear, which leads to a non-linear relationship between the accuracy and the number of sensors used [26]. Consequently, using more sensors does not always improve the localization performance.

Furthermore, the geometry structure of the sensor-emitter network is also an important factor [27] and the sensors selected should be distributed around the emitter [28]. The distribution structure of the sensors with a uniform angular separation around the emitter is the geometric structure [27]. A successful geometry structure can be established by selecting sensors from different spatial directions of the emitter. However, the emitter is not always located in the center of the sensing area, it may locate on the boundaries of the sensing area. To select the sensors spaced around the emitter, we divide the sensing area into multiple equiangular partitions and examine whether there is at least one sensor in each partition.

The selection algorithm is described in detail in the following. First, due to the unknown emitter location, m ($m < N$) random sensors measure the RSS values and report the measurements to the FC. Using the localization method provided in Sec. 3, we perform the first estimation and obtain an initial emitter location (i.e., X_1). Then, depending on the number of sensors (i.e., M) required in the second estimation, we divide the sensing area with the center of X_1 into M partitions equally in the polar angle domain. The M partitions are numbered clockwise or counterclockwise by partition i, $i = 1, \cdots, M$, where clockwise or counterclockwise numbering yields similar results. Subsequently, we proceeded with the analysis in a counterclockwise fashion. For two neighboring partitions I and J ($I < J$), a sensor on the boundary of the two partitions is considered to be in partition I. Finally, we search for the sensor closest to the emitter in each partition in turn. When there is an empty partition, the empty partition will be skipped and its number will be recorded until all partitions are traversed. We record the number of these empty partitions as e. The e empty partitions are renumbered counterclockwise by partition ii, $ii = 1, \cdots, e$.

For the e empty partitions, we first select the nearest e sensors to the emitter among the set of unselected sensors. The e sensors are denoted by S_{ii}, $ii = 1, \ldots, e$. The distances of e sensors to the emitter are denoted as D_{ii}, $ii = 1, \ldots, e$. If two sensors are equal in distance from the emitter, their RSS values are similar. From this aspect, we deduce that there is a point of the length equal to D_{ii} on the angle bisector of the empty partition ii. The e locations are denoted by S_{ii}^*. Then, we express the RSS measurements at coordinate S_{ii}^* by using the RSSs at the S_{ii}. We refer to these points as

simulated sensor nodes. Specifically, these simulated sensors are imaginary, and their information can only be inferred by S_{ii}. We give the inference process in the following.

The coordinates of sensors S_{ii} are converted into a polar coordinate system. The polar coordinates of the e real and simulated sensors are denoted by (r_{ii},ρ_{ii}) and (r^*_{ii},ρ^*_{ii}), for $ii = 1, \ldots, e$, where $r^*_{ii} = r_{ii}$, $\rho^*_{ii} = (2\pi i - \pi)/M$, and i is the initial number of the empty partition. Thus, we obtain the Cartesian coordinates of the simulated sensors given by $(r^*_{ii}\cos(\rho^*_{ii}), r^*_{ii}\sin(\rho^*_{ii}))$. More sensors are deployed to avoid too many empty partitions. In addition, when there are more empty partitions, all partitions are rotated around the emitter location. The rotation acts like a re-division of the area.

When all partitions have available sensors, all selected sensors are activated to perform measurement. The measured data are then transferred to FC to perform the second refined estimation. An example without empty partitions is given, as shown in Fig. 2(a). An example with one empty partition is shown in Fig. 2(b), where the simulated sensor is inferred by the fifth sensor. Figure 3 details the process of the sensor selection method.

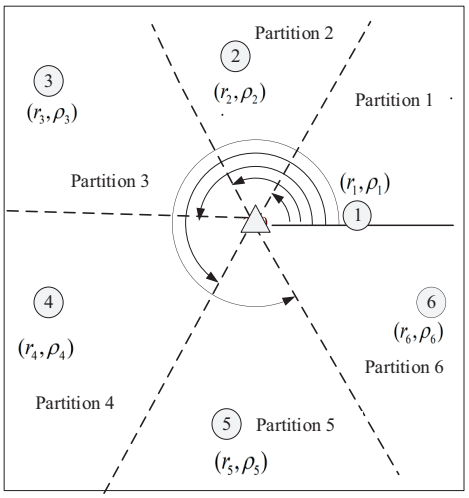

(a) Sensing area splitting with 6 partitions and sensor locations

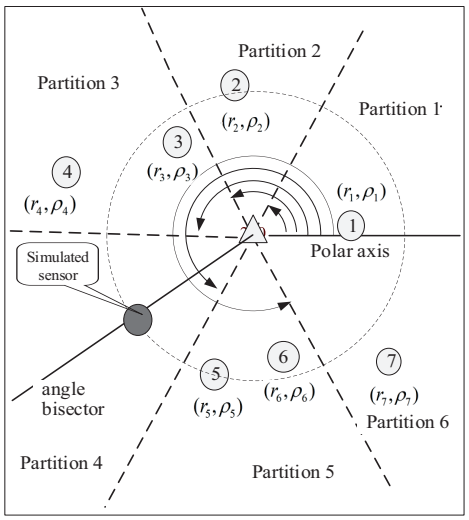

(b) Sensing area splitting with one empty partition

Fig. 2. Sensing area partition.

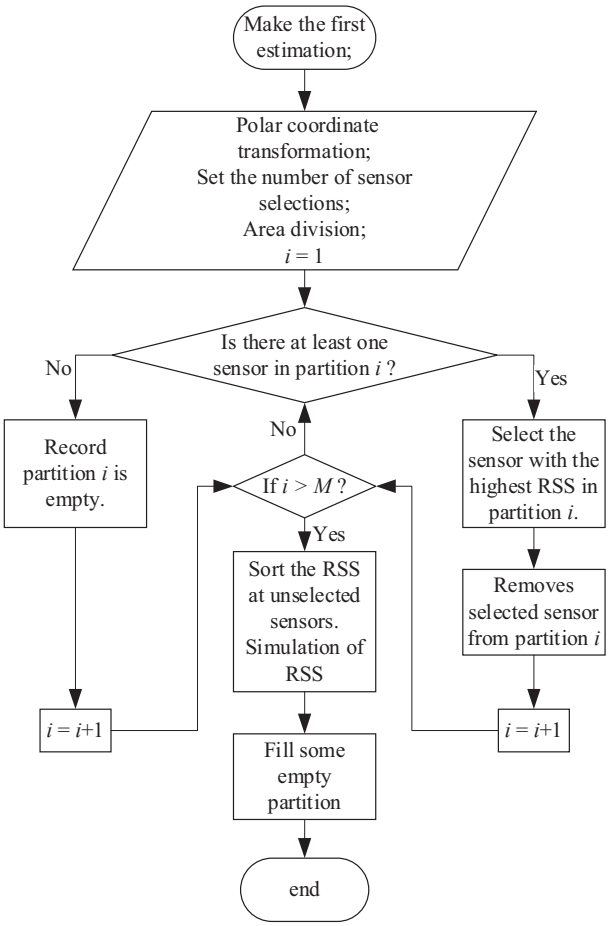

Fig. 3. Flow chart of the proposed sensor selection method.

4.2 Algorithm Framework

With sensor selection, the localization algorithm needs to be executed twice. In the first step, m random deployed sensors are used to passively measure the RSSs from the emitter and report the values to FC. The initial location estimate is obtained by performing the first estimation using the sensed RSS measurements based on SDP as in Sec. 3. According to the initial estimation and selection algorithm, other M sensors are selected to actively measure RSSs. Then a second estimation step is executed at the FC to give a more accurate result. Figure 4 depicts the flow of the localization.

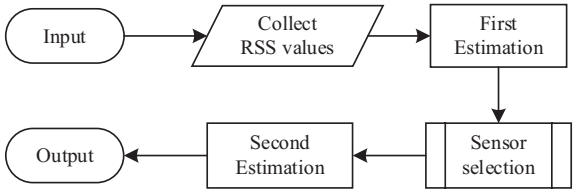

Fig. 4. Framework of the RSS-based localization algorithm.

5. Simulation Results and Analysis

5.1 Simulation Settings

In this section, two optimization schemes presented in [13] and [17] are compared to validate the proposed algorithm (denoted by "SS-SDP"). The two counterpart schemes are represented by "SOCP-random" and "LSRE-random", respectively. The results are also compared with the CRLB, which is widely used to represent the lower bound of an unbiased estimator. All of the mentioned algorithms were solved using the MATLAB R2020a package CVX [29]. The times were captured by a laptop with an AMD R7-5800H 3.3 GHz CPU and 16 GB RAM.

In the simulated scenario, 100 known sensors are deployed in a 2-D area, with 50 sensors randomly distributed within the area and the remainder uniformly distributed on the boundary of the area. We assume that the sensors are equipped with omnidirectional antennas [16]. As the sensors are fixed and will work for a long period of time, we simply choose the more stable sensors. The emitter is randomly placed in this area. Figure 5 represents a scenario with 30 sensors and an emitter. The PLE is taken as a known parameter, unless otherwise stated. Our experimental environment is line-of-sight. Only the environmental noise and path loss are considered in the information transmission. The propagation model in (1) is employed to generate the RSS measurements. The shadowing variables n_i is generated using a Gaussian distribution $\mathcal{N}(0, \sigma_i^2)$ with consistent variances $\sigma_i^2 = \sigma$ for $i = 1, \ldots, N$. The root mean square error (RMSE) is used to measure the localization performance, and is defined by:

$$\mathrm{RMSE} = \sqrt{\frac{1}{Mc}\sum_{i=1}^{Mc}\left\|X_i - \widehat{X}_i\right\|^2} \tag{18}$$

where Mc represents the number of Monte Carlo (Mc) runs. X_i and $\widehat{X}_i$ are the true emitter location and the estimated location in the i-th run, respectively. The simulation parameters are shown in Tab. 1.

In our simulations, the proposed algorithm invokes $m = 5$ sensors randomly to passively sample the radio signals and perform the initial estimation. Then we select $M = 13$ sensors to actively measure the RSSs and perform the second estimation. The other two algorithms to be compared also use 13 sensors randomly to perform the localization. To verify the effect of unknown P_0 on the estimated performance, we set $\sigma = 3$ and select M sensors.

Parameter	Value
Field dimension	100×100 m^2
Transmitted power at d_0 (P_0)	(–20, –10, 10, 20, 30, 40) dBm
Reference distance (d_0)	1 m
Path loss exponent (β)	4
Standard deviation (σ)	1, 2, 3, 4, 5, 6
Number of samples (N_j)	100
Monte Carlo runs (Mc)	3000

Tab. 1. Model simulation parameter values.

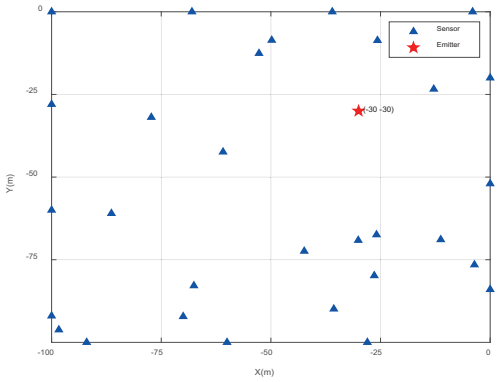

Fig. 5. Scenario with 30 sensors and one emitter.

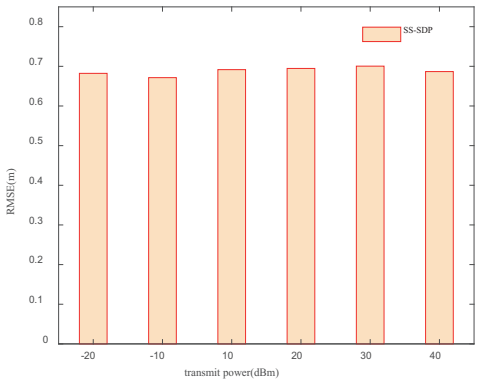

Fig. 6. RMSE at different P_0.

The RMSE data for different transmitted powers are recorded as shown in Fig. 6. It can be seen that the RMSE is independent of the P_0. Thus, in the following, we select the transmitted power arbitrarily.

5.2 Sensor Selection Simulation Results

To verify the importance of sensor selection, 10, 20, 30, 40, 50, and 60 sensors are selected respectively to perform the three localization algorithms in the scenario with σ = 3 dB. Figure 7 shows the impact of the number of sensors on RMSE of the emitter location estimation. The results indicate that the proposed SS-SDP performs well with different numbers of sensors. The RMSE decreases as

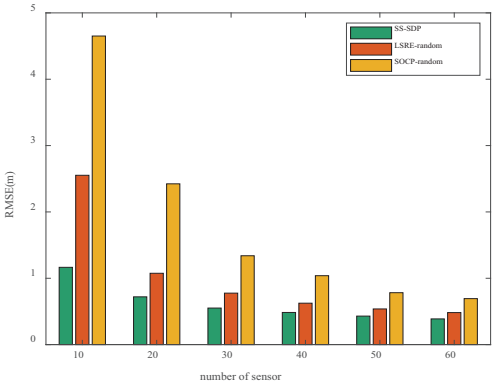

Fig. 7. RMSE performances with different numbers of sensors.

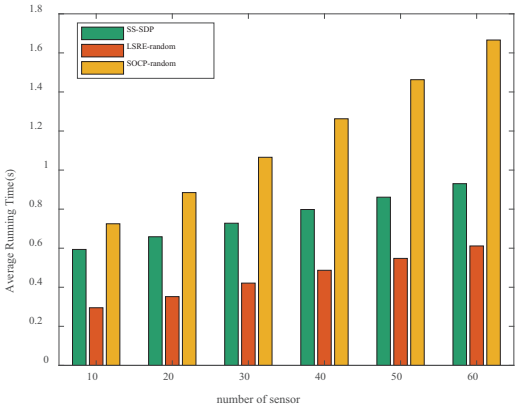

Fig. 8. Impacts of number of sensors on average running time.

the number of sensors increases. The average running time of the algorithm is shown in Fig. 8. It shows using more sensors will increase the running time of the algorithm. Figures 7 and 8 also show that it takes a longer time with more sensors while the localization accuracy is slightly increased. The proposed algorithm performs well when fewer sensors are selected. The gains from the algorithm are not optimal when more sensors are selected.

5.3 Impact of Standard Deviation of Shadowing Effect on RMSE

We then investigate the scenario with varying shadowing levels. In this scenario, the number of sensors used is fixed as 13 (i.e., M = 13). The RMSE curves for the considered algorithms are given in Fig. 9. In general, the RMSE and the CRLB increase with σ. The gap between the RMSE of the SS-SDP and the LSRE-random is larger than 0.4. As σ increases, the RMSE gap between the two algorithms increases. Moreover, Figure 9 shows that the RMSE growth rate of SS-SDP slows down. LSRE-random has a significant performance improvement over the SOCP-random. The RMSE curves for the estimated transmit power are shown in Fig. 10. The results in Fig. 9 and 10 show that SS-SDP has higher accuracy for both the location and transmit power estimations. Notably, the variation range of RMSE of SS-SDP is the smallest. Hence, SS-SDP results in the lowest sensitivity to channel shadowing.

With σ = 3 and M = 13, we find a threshold value of m. The range of m is from 3 to 6. The results of the two estimations are shown in Tab. 2. According to Tab. 2, the final results do not outperform the LSRE-random algorithm at m = 3 or 4. But when m is bigger than 5, the result is better than that of LSRE-random algorithm.

First estimation				
m	3	4	5	6
RMSE	11.29	9.29	5.38	3.87
Second estimation				
RMSE	2.17	1.79	0.68	0.61

Tab. 2. RMSE for the two estimations.

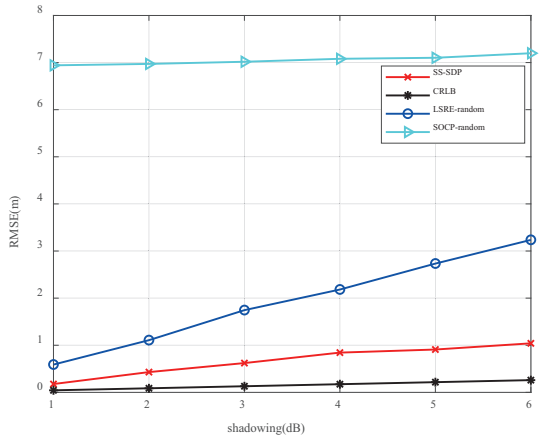

Fig. 9. RMSE of the location estimation versus σ.

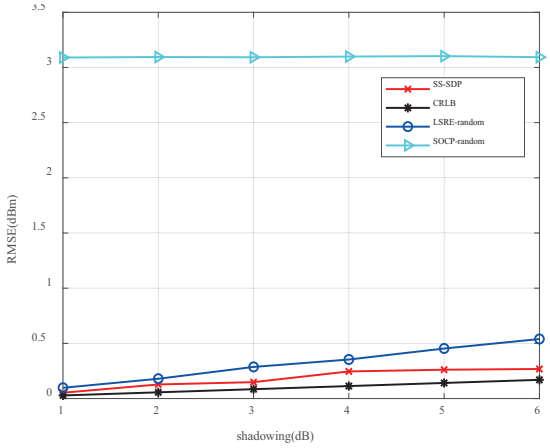

Fig. 10. RMSE of the transmit power estimation versus σ.

5.4 Impact of the Number of Sensors on RMSE

With a fixed σ = 3 dB, we examine the localization performance for different numbers of sensors, with M varying between 8 and 18. The RMSE of the emitter location estimates versus the number of sensors is shown in Fig. 11. The result shows that the CRLB and the RMSE decrease as the number of sensors increases. The SS-SDP algorithm still outperforms the other two algorithms. When M = 8, the SS-SDP performs roughly 60% and 70% better than the LSRE-random and SOCP-random algorithms, respectively. As the number of sensors increases, the RMSE gap between the LSRE-random and the SS-SDP decreases.

To further validate the performance of the SS-SDP, we estimate the location with a different number of sensors while keeping the RMSE between 0.90 and 1.00. Table 3 shows the relationship between the number of sensors involved in localization and the RMSE of location estimation. Therefore, the SS-SDP uses about 1/2 of the LSRE-random and about 1/7 of the SOCP-random in terms of the number of sensors to achieve similar performance. It significantly indicates the superiority of the SS-SDP algorithm.

Algorithm	Number	Accuracy
SS-SDP	Selecting 8 or 9 sensors	0.91~0.97
LSRE-random	Randomly selecting 20 or 21 sensors	0.94~0.98
SOCP-random	Randomly selecting 75 or 76 sensors	0.91~0.97

Tab. 3. The number of sensors versus RMSE.

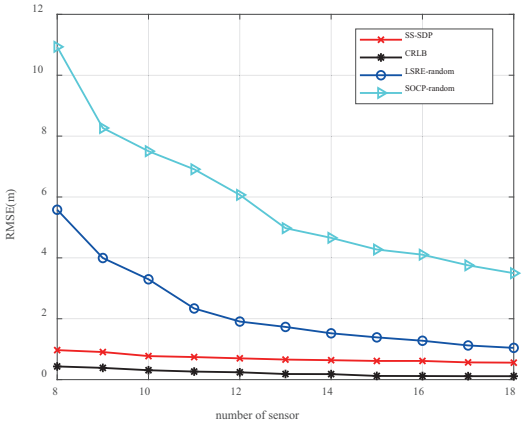

Fig. 11. RMSE of location estimation versus the number of sensors.

Algorithm	Complexity
SS-SDP	$\mathcal{O}\left(\sqrt{(M+k)}\left(M+k^2\right)^3\right)$
LSRE-random	$\mathcal{O}\left(\sqrt{(M+k)}\left(M+k^2\right)^3\right)$
SOCP-random	$2\mathcal{O}\left(M^{3.5}\right)$

Tab. 4. Computational complexity. (Note: The number of sensors and the localization dimension are denoted by M and k, respectively.)

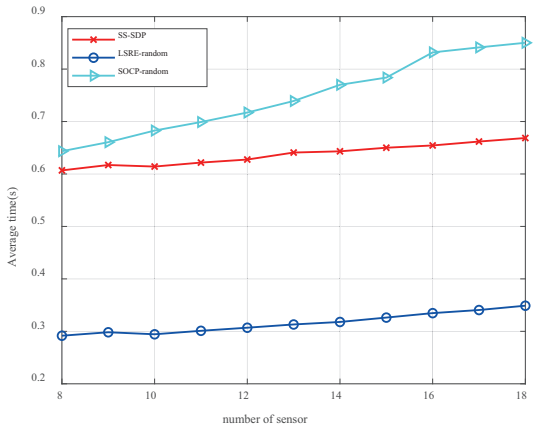

Fig. 12. Average running time versus the number of sensors.

Computational complexity is also an important factor that affects the performance of the algorithm. The trade-off between estimation accuracy and complexity is also investigated and the complexities of the considered algorithms are summarized in Tab. 4.

The average running time as the number of sensors varies is shown in Fig. 12. The results reveal that the average running time of the LSRE-random is about 2 to 3 times that of the SOCP-random. The SS-SDP performs twice in our scheme, so it takes more time than the LSRE-random. The results in Fig. 12 and Tab. 4 match well. We conclude that the SS-SDP achieves better performance with relatively low complexity.

5.5 Localization Error versus Emitter Location

In this experiment, the locations of the emitter are changed, the effects of the location on the estimation performance are investigated. The emitter location is assumed to vary from the center to the edge of the sensing area. Typical locations are (–60, –60), (–70, –70), (–80, –80), and (–90, –90). The results of the RMSE are plotted in Fig. 13.

It is shown that the RMSE of the three methods increases gradually as the emitter moves from the center of the area to the boundary. The SS-SDP algorithm has the smallest RMSE increment and shows the best performance in the central area. When only 8 sensors are employed, the

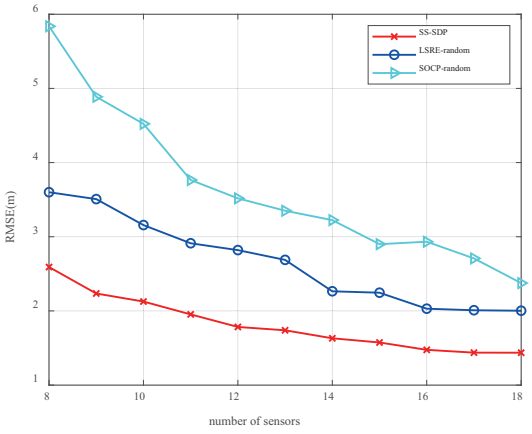

(a)

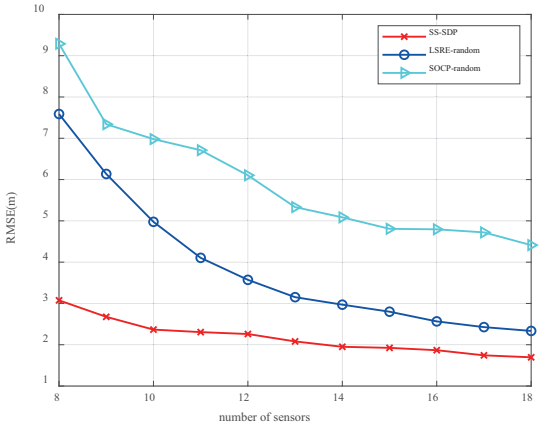

(b)

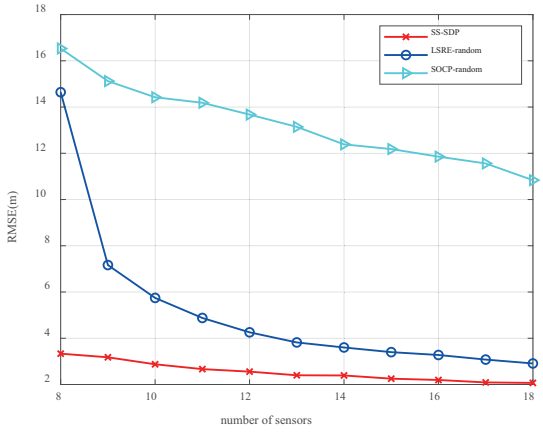

(c)

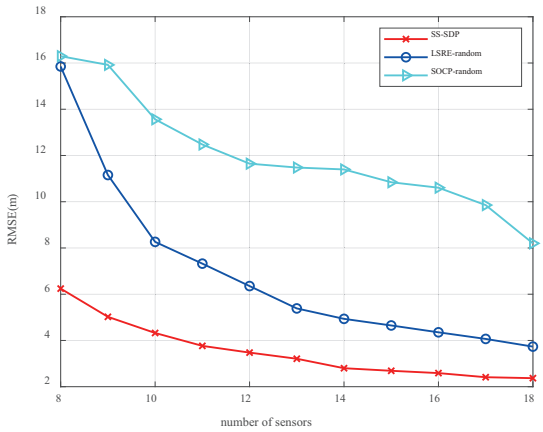

(d)

Fig. 13. Localization errors versus emitter location. (a), (b), (c), and (d) represents the corresponding RMSE of location estimation under the four locations of (–60, –60), (–70, –70), (–80, –80), and (–90, –90).

RMSE of the SS-SDP grows from 2.8 m to around 6 m for the four locations. When there are more than 12 sensors, the RMSE of the SS-SDP algorithm remains below 3 m. Therefore, the SS-SDP algorithm effectively alleviates the performance degradation caused by the emitter location changes.

6. Conclusion

We have proposed an uncooperative emitter localization method based on joint sensor selection and semidefinite programming optimization to increase the accuracy in RSS-based localization and to lower computation complexity. The superiority of the algorithm has been demonstrated through extensive simulations, compared to other typical localization methods. We show that in future IoT or WSN localization scenarios with massive radio frequency sensors, sensor selection is a critical step in lowering the algorithm complexity and the energy consumption. In future work, a more practical path loss model for the non-line-of-sight propagation should be considered and the investigated joint optimization approach in this study will be extended to the new scenario.

Acknowledgments

This research of this paper was supported by the National Natural Science Foundation of China under Grant 62131005, 61901497 and 61801231.

References

[1] ZAFARI, F., GKELIAS, A., LEUNG, K. A survey of indoor localization systems and technologies. *IEEE Communications Surveys & Tutorials*, 2019, vol. 21, no. 3, p. 2568–2599. DOI: 10.1109/COMST.2019.2911558

[2] VERA-AMARO, R., RIVERO-ANGELES, M. E., LUVIANO-JUAREZ, A. Design and analysis of wireless sensor networks for animal tracking in large monitoring polar regions using phase-type distributions and single sensor model. *IEEE Access*, 2019, vol. 7, p. 45911–45929. DOI: 10.1109/ACCESS.2019.2908308

[3] YAN, Y., YANG, G., WANG, H., et al. Semidefinite relaxation for source localization with quantized ToA measurements and transmission uncertainty in sensor networks. *IEEE Transactions on Communications*, 2021, vol. 69, no. 2, p. 1201–1213. DOI: 10.1109/TCOMM.2020.3037551

[4] KATWE, M., GHARE, P., SHARMA, P. K., et al. NLOS error mitigation in hybrid RSS-TOA-based localization through semidefinite relaxation. *IEEE Communications Letters*, 2020, vol. 24, no. 12, p. 2761–2765. DOI: 10.1109/LCOMM.2020.3020948

[5] VELASCO, J., PIZARRO, D., MACIAS-GUARASA, J., et al. TDOA matrices: Algebraic properties and their application to robust denoising with missing data. *IEEE Transactions on Signal Processing*, 2016, vol. 64, no. 20, p. 5242–5254. DOI: 10.1109/TSP.2016.2593690

[6] MINGYI, Y., ANNAN, L. A robust TDOA based solution for source location using mixed Huber loss. *Journal of Systems Engineering and Electronics*, 2021, vol. 32, no. 6, p. 1375–1380. DOI: 10.23919/JSEE.2021.000117

[7] WANG, Y., HO, K. C. Unified near-field and far-field localization for AOA and hybrid AOA-TDOA positionings. *IEEE Transactions on Wireless Communications*, 2018, vol. 17, no. 2, p. 1242–1254. DOI: 10.1109/TWC.2017.2777457

[8] ZHENG, Y., SHENG, M., LIU, J., et al. Exploiting AoA estimation accuracy for indoor localization: A weighted AoA-based approach. *IEEE Wireless Communications Letters*, 2019. vol. 8, no. 1, p. 65–68. DOI: 10.1109/LWC.2018.2853745

[9] POLAK, L., ROZUM, S., SLANINA, M., et al. Received signal strength fingerprinting-based indoor location estimation employing machine learning. *Sensors (Basel)*, 2021, vol. 21, no. 13, p. 4605–4629. DOI: 10.3390/s21134605

[10] ALTAF KHATTAK, S. B., FAWAD, NASRALLA, M. M., et al. WLAN RSS-based fingerprinting for indoor localization: A machine learning inspired bag-of-features approach. *Sensors (Basel)*, 2022, vol. 22, no. 14, p. 5236–5251. DOI: 10.3390/s22145236

[11] ZOU, Y., LIU, H. RSS-based target localization with unknown model parameters and sensor position errors. *IEEE Transactions on Vehicular Technology*, 2021, vol. 70, no. 7, p. 6969–6982. DOI: 10.1109/TVT.2021.3089161

[12] WANG, Z. F., ZHANG, H., LU, T., et al. Cooperative RSS-based localization in wireless sensor networks using relative error estimation and semidefinite programming. *IEEE Transactions on Vehicular Technology*, 2019, vol. 68, no. 1, p. 483–497. DOI: 10.1109/TVT.2018.2880991

[13] SHI, J., WANG, G., JIN, L. Least squared relative error estimator for RSS based localization with unknown transmit power. *IEEE Signal Processing Letters*, 2020, vol. 27, p. 1165–1169. DOI: 10.1109/LSP.2020.3005298

[14] DOGANDZIC, A., JIN, J. H. Maximum likelihood estimation of statistical properties of composite gamma-lognormal fading channels. *IEEE Transactions on Signal Processing*, 2004, vol. 52, no. 10, p. 2940–2945. DOI: 10.1109/TSP.2004.834265

[15] ZISKIND, I., WAX, M. Maximum likelihood localization of multiple sources by alternating projection. *IEEE Transactions on Acoustics, Speech, and Signal Processing*, 1988, vol. 36, no. 10, p. 1553–1560. DOI: 10.1109/29.7543

[16] WANG, G., CHEN, H., LI, Y., et al. On received-signal-strength based localization with unknown transmit power and path loss exponent. *IEEE Wireless Communications Letters*, 2012, vol. 1, no. 5, p. 536–539. DOI: 10.1109/WCL.2012.072012.120428

[17] VAGHEFI, R. M., GHOLAMI, M. R., BUEHRER, R. M., et al. Cooperative received signal strength-based sensor localization with unknown transmit powers. *IEEE Transactions on Signal Processing*, 2013, vol. 61, no. 6, p. 1389–1403. DOI: 10.1109/TSP.2012.2232664

[18] TOMIC, S., BEKO, M., DINIS, R. RSS-based localization in wireless sensor networks using convex relaxation: Noncooperative and cooperative schemes. *IEEE Transactions on Vehicular Technology*, 2015, vol. 64, no. 5, p. 2037–2050. DOI: 10.1109/TVT.2014.2334397

[19] ABABNEH, A. A. Density-based sensor selection for RSS target localization. *IEEE Sensors Journal*, 2018, vol. 18, no. 20, p. 8532–8540. DOI: 10.1109/JSEN.2018.2866062

[20] ABABNAH, A., NATARAJAN, B. Optimal control-based strategy for sensor deployment. *IEEE Transactions on Systems, Man, and Cybernetics - Part A: Systems and Humans*, 2011, vol. 41, no. 1, p. 97–104. DOI: 10.1109/TSMCA.2010.2049992

[21] BOPARDIKAR, S. D., ENNASR, O., TAN, X. Randomized sensor selection for nonlinear systems with application to target localization. *IEEE Robotics and Automation Letters*, 2019, vol. 4, no. 4, p. 3553–3560. DOI: 10.1109/LRA.2019.2928208

[22] BEL, A., VICARIO, J. L., SECO-GRANADOS, G. Node selection for cooperative localization: Efficient energy vs. accuracy tradeoff. In *IEEE 5th International Symposium on Wireless Pervasive Computing 2010*. Modena (Italy), 2010, p. 307–312. DOI: 10.1109/ISWPC.2010.5483734

[23] DAI, Z., WANG, G., JIN, X., et al. Nearly optimal sensor selection for TDOA-based source localization in wireless sensor networks. *IEEE Transactions on Vehicular Technology*, 2020, vol. 69, no. 10, p. 12031–12042. DOI: 10.1109/TVT.2020.3011118

[24] YILMAZ, H. B., TUGCU, T. Location estimation-based radio environment map construction in fading channels. *Wireless Communications & Mobile Computing*, 2015, vol. 15, no. 3, p. 561–570. DOI: 10.1002/wcm.2367

[25] MUKHOPADHYAY, B., SRIRANGARAJAN, S., KAR, S. Signal strength-based cooperative sensor network localization using convex relaxation. *IEEE Wireless Communications Letters*, 2020, vol. 9, no. 12, p. 2207–2211. DOI: 10.1109/LWC.2020.3018679

[26] ABABNEH, A. A. Knapsack-based sensor selection for target localization under energy and error constraints. *IEEE Sensors Journal*, 2021, vol. 21, no. 23, p. 27208–27217. DOI: 10.1109/JSEN.2021.3123734

[27] BISHOP, A. N., JENSFELT, P. An optimality analysis of sensor-target geometries for signal strength based localization. In *2009 International Conference on Intelligent Sensors, Sensor Networks and Information Processing (ISSNIP)*. Melbourne (VIC, Australia), 2009, p. 127–132. DOI: 10.1109/ISSNIP.2009.5416784

[28] HAVYARIMANA, V., XIAO, Z., SIBOMANA, A., et al. A fusion framework based on sparse Gaussian–Wigner prediction for vehicle localization using GDOP of GPS satellites. *IEEE Transactions on Intelligent Transportation Systems*, 2020, vol. 21, no. 2, p. 680–689. DOI: 10.1109/TITS.2019.2891585

[29] GRANT, M., BOYD, S. *CVX: MATLAB Software for Disciplined Convex Programming.* [Online] Cited 2021-02-23. Available at: http://cvxr.com/cvx

About the Authors …

Liming CAO is currently a master student at the School of Electronics and Information Engineering, Nanjing University of Information Science and Technology, Nanjing, China. His research interests include wireless sensor network communication and localization based on received signal strength.

Jianzhao ZHANG received the Ph.D. degree in Communication Engineering from the PLA University of Science and Technology, Nanjing, China, in 2012. He is currently a senior engineer in the Sixty-Third Research Institute, National University of Defense Technology, Nanjing, China. His research interests include wireless communications, and dynamic spectrum management.

Yongxiang LIU (corresponding author: The Sixty-Third Research Institute, National University of Defense Technology, Nanjing, China, 210007) received the M.S. degree in Communications and Information Systems from the Institute of Communications Engineering, Nanjing, China, in 1999. He is currently a Professor in the Sixty-Third Research Institute, National University of Defense Technology, Nanjing, China. His research interests include wireless communications, spectrum management, and communication anti-jamming.

Yanping ZHU received the Ph.D. degree in Information and Communication Engineering from Nanjing University of Science and Technology, China, 2014. She is currently working as a lecturer at Nanjing University of Information Science and Technology, Nanjing, China. She worked as an academic visitor in University of Sheffield, UK, 2018. Her research interests include MIMO radar/communication spectrum sharing and intelligent signal processing.

Junquan DENG received the B.Eng. degree in Automation Engineering from Tsinghua University, Beijing, China, in 2011, the M.Sc. degree in Computer Science from the National University of Defense Technology (NUDT), Changsha, China, in 2013, and the Ph.D. degree in Information Theory from Aalto University, Aalto, Finland, in 2018. Since 2019, he is an Assistant Research Fellow with the Sixty-Third Research Institute, National University of Defense Technology, Nanjing, China. His research interests include device-to-device communication, millimeter-wave communication, mobile relaying in 5G cellular networks, and machine learning with wireless network data.

Guokai CHEN received a B.S degree in Measurement and Control Technology from the National University of Defense Technology in 2019. He is currently a Ph.D. student in the College of Intelligence Science at the National University of Defense Technology. His research interests include radio map construction methods and radio map-based localization.

Appendix: Cramer-Rao Lower Bound

The Cramer-Rao lower bound (CRLB) is defined as a lower bound on the variance of any unbiased estimator and is widely used as a benchmark for localization performance. The CRLB for RSS-based localization had been derived in [17] and [18]. It was derived from the inverse matrix of Fisher's information matrix. A concise derivation process is given below. From the measurement model in (1), the probability density function of the RSS measurements is written as [17]:

$$p(F;\widehat{\theta}) = \prod_{i=1}^{M} \frac{1}{\sqrt{2\pi\sigma^2}} \exp\left\{ -\frac{\left(P_i - P_0 + 10\beta \log_{10}\left(d_i\right)\right)^2}{2\sigma^2} \right\} \quad (19)$$

where the matrix $F = \left[P_1, \cdots, P_M\right]^{\mathrm{T}}$ represents the signal strength values. M indicates the number of sensors.

Taking the logarithm of both sides of (19), we obtain:

$$\ln p(F;\widehat{\theta}) = -\frac{M}{2}\ln\left(2\pi\sigma^2\right) - \frac{1}{2\sigma^2}\sum_{i=1}^{M}\left(P_i - P_0 + 10\beta\log_{10}\left(d_i\right)\right)^2 . \quad (20)$$

The first-order and second-order partial derivatives of (20) are taken respectively. We then apply them to form the Fisher information matrix $I\left(\widehat{\theta}\right)$:

$$I\left(\widehat{\theta}\right)_{ij} = -E\left[\frac{\partial^2 \ln p(F;\widehat{\theta})}{\partial\widehat{\theta}_i \partial\widehat{\theta}_j}\right] i = 1,2,3;\ j = 1,2,3 . \quad (21)$$

Following (20) and (21), the $I\left(\widehat{\theta}\right)$ can be written as:

$$I\left(\widehat{\theta}\right) = -\begin{bmatrix} E\left(\frac{\partial^2 \ln p(F;\widehat{\theta})}{\partial a^2}\right) & E\left(\frac{\partial^2 \ln p(F;\widehat{\theta})}{\partial a \partial b}\right) & E\left(\frac{\partial^2 \ln p(F;\widehat{\theta})}{\partial a \partial P_0}\right) \\ E\left(\frac{\partial^2 \ln p(F;\widehat{\theta})}{\partial b \partial a}\right) & E\left(\frac{\partial^2 \ln p(F;\widehat{\theta})}{\partial b^2}\right) & E\left(\frac{\partial^2 \ln p(F;\widehat{\theta})}{\partial b \partial P_0}\right) \\ E\left(\frac{\partial^2 \ln p(F;\widehat{\theta})}{\partial P_0 \partial a}\right) & E\left(\frac{\partial^2 \ln p(F;\widehat{\theta})}{\partial P_0 \partial b}\right) & E\left(\frac{\partial^2 \ln p(F;\widehat{\theta})}{\partial P_0^2}\right) \end{bmatrix} . \quad (22)$$

The diagonal elements of the inverse of the Fisher information matrix $I^{-1}\left(\widehat{\theta}\right)$ are the CRLB of the unknown parameters.